Sensors and Actuators B 230 (2016) 600–606

Contents lists available at ScienceDirect

Sensors and Actuators B: Chemical

journal homepage: www.elsevier.com/locate/snb

3-D printed adjustable microelectrode arrays for electrochemical sensing and biosensing

Haipeng Yang[a,b,1], Md Taibur Rahman[a,1], Dan Du[a], Rahul Panat[a,*], Yuehe Lin[a,*]

[a] School of Mechanical and Material Engineering, Washington State University, Pullman, WA 99164, United States
[b] College of Materials Science and Engineering, Nanshan District Key Lab for Biopolymers and Safety Evaluation, and Shenzhen Key Laboratory of Special Functional Materials, Shenzhen University, Shenzhen 518060, PR China

ARTICLE INFO

Article history:
Received 3 December 2015
Received in revised form 9 February 2016
Accepted 22 February 2016
Available online 26 February 2016

Keywords:
Microelectrode arrays
Micro additive manufacturing
Hydrogen peroxide
Electrochemical sensor
Biosensor

ABSTRACT

Printed electronics has emerged as an important fabrication technique that overcomes several shortcomings of conventional lithography and provides custom rapid prototyping for various sensor applications. In this work, silver microelectrode arrays (MEA) with three different electrode spacing were fabricated using 3-D printing by the aerosol jet technology. The microelectrodes were printed at a length scale of about 15 μm, with the space between the electrodes accurately controlled to about 2 times (30 μm, MEA30), 6.6 times (100 μm, MEA100) and 12 times (180 μm, MEA180) the trace width, respectively. Hydrogen peroxide and glucose were chosen as model analytes to demonstrate the performance of the MEA for sensor applications. The electrodes are shown to reduce hydrogen peroxide with a reduction current proportional to the concentration of hydrogen peroxide for certain concentration ranges. Further, the sensitivity of the current for the three electrode configurations was shown to decrease with an increase in the microelectrode spacing (sensitivity of MEA30:MEA100:MEA180 was in the ratio of 3.7:2.8:1), demonstrating optimal MEA geometry for such applications. The noise of the different electrode configurations is also characterized and shows a dramatic reduction from MEA30 to MEA100 and MEA180 electrodes. Further, it is shown that the response current is proportional to MEA100 and MEA180 electrode areas, but not for the area of MEA30 electrode (the current density of MEA30:MEA100:MEA180 is 0.25:1:1), indicating that the MEA30 electrodes suffer from diffusion overlap from neighboring electrodes. The work thus establishes the lower limit of microelectrode spacing for our geometry. The lowest detection limit of the MEAs was calculated (with $S/N = 3$) to be 0.45 μM. Glucose oxidase was immobilized on MEA100 microelectrodes to demonstrate a glucose biosensor application. The sensitivity of glucose biosensor was 1.73 μA mM^{-1} and the calculated value of detection limit ($S/N = 3$) was 1.7 μM. The electrochemical response characteristics of the MEAs were in agreement with the predictions of existing models. The current work opens up the possibility of additive manufacturing as a fabrication technique for low cost custom-shaped MEA structures that can be used as electrochemical platforms for a wide range of sensor applications.

1. Introduction

An array of microelectrodes (MEA) shows many advantages over a conventional (individual) microelectrode such as increased mass transport, fast response times, decreased influence of the solution resistance, enhanced sensitivities, and the lower limit of detection (LOD) [1–3]. Further, studies have shown that individual microelectrodes show high mass-transfer flux and a low value of the potential drop, but have a very low current carrying capability due to the low cross section area. The MEAs are shown to increase the current carrying capability while maintaining the advantages of a single microelectrode with respect to mass diffusion and ohmic drop [4]. Each microelectrode of an MEA, however, has a diffusion layer associated with it. In order to make each electrode work as an individual microelectrode, the spacing between electrodes (for a given electrode width) in an MEA needs to be sufficiently large to avoid the diffusion layer overlap with the adjacent electrodes [5,6]. Since the noise level depends on the dimension of the individual electrodes whereas the signal strength depends on the total surface area of the electrodes, the size reduction of each

* Corresponding authors.
E-mail addresses: rahul.panat@wsu.edu (R. Panat), yuehe.lin@wsu.edu, yuehe.lin@pnnl.gov (Y. Lin).
[1] These authors contributed equally to this work.

http://dx.doi.org/10.1016/j.snb.2016.02.113
0925-4005/

individual electrode and the increase of the total number of electrodes, as in an MEA, is shown to improve the signal-to-noise (*S*/*N*) ratio and achieve lower LOD [5,7]. An excellent sensor action can be obtained by controlling the space between each microelectrode of MEAs to achieve maximum number of electrodes and avoid the overlap of the diffusion layer, while using the individual microelectrode for the sensing action.

Previously, lithography, template methods, or chemical self-assembly were explored to fabricate micro/nanoelectrode arrays [8–12]. Such methods typically involve the use of harmful chemicals, multiple fabrication steps and create material waste [13,14]. In addition, the material choices for sensor platforms are rather restricted due to the substrate compatibility with the chemical processes used. Lastly, a need for customized biosensors to each individual is emerging in specific applications which requires rapid changes in sensor circuitry to change the detection range and/or limit. The above fabrication techniques are not suitable for such rapid and customized changes to circuitry without resulting in a significant cost increase. Recently, direct write 3-D printing has become a valuable technique in a wide variety of applications, such as chemistry reaction container [15,16], microfluidics [17], sensors [18], photodetectors [19], graphene interconnects [20], and biomimetic structures [21]. However, few works have been achieved on the fabrication of microelectrode arrays with 3D printing technique [22]. The direct write printing method can 'write' microelectronic circuit on any surface without requiring the use of harmful chemicals and without creating material waste [23,24]. In addition to being scalable, this technique can allow rapid and customized changes to sensor design. Lastly, direct-write techniques can create sensors on any substrate as long as the substrate is hydrophilic and it allows highly complex/dense metal-polymer circuitry required for the electrochemical detection.

In this paper, we report design and direct-write fabrication of MEAs with adjustable array spacing as a platform for electrochemical sensing. The space between microelectrodes of the three fabricated MEAs is controlled to be 30, 100, and 180 μm, respectively. By using direct write 3D printing technique, it is easy to find the minimum spacing between electrodes on MEAs to get the maximum signal-to-noise (*S*/*N*) ratio. Sensor performance is demonstrated through the detection of hydrogen peroxide and glucose, chosen as model analytes. The sensitivity and accuracy of detection was determined as a function of the printed MEA structure geometry. The potential applications of this method for other types of electrochemical sensors are also discussed.

2. Experimental

2.1. Micro-electrode array fabrication

The MEAs were fabricated using aerosol jet (AJ) based direct-write technology that allows deposition of solvent based nanoparticles with solution viscosity ranging from 1 to 1000 cP. A schematic of the AJ system (AJ 300, Optomec Inc., Albuquerque, NM, USA) is shown in Fig. 1 and includes two atomizers (ultrasonic and pneumatic), a programmable XY motion stage, and a deposition head. Solvent based nanoparticle ink is placed in the atomizer which creates a continuous and dense mist of nanoparticles with a droplet size of 1–5 μm which is then transferred to the deposition head with the help of a carrier gas N_2. The mist or dense vapor is then focused and driven towards the nozzle with the help of a secondary gas (also N_2) to form a micro-jet. A UV apparatus (UJ35 UV cure subsystem, Panasonic Corporation, Osaka, Japan) connected to the machine can instantaneously cure the (UV curable) polymer. Primary materials used to fabricate the biosensor were silver nanoparticle ink (Perfect-TPS 40 G2, Clariant Group, Frankfurt, Germany) and a UV curable polymer (Loctite 3105, Henkel Corporation, Düsseldorf, Germany). The silver nanoparticles had a size of about 30–50 nm with about 40 ± 2 wt% particle loading in the ink and a viscosity of about 1.5 cP according to the manufacturer data sheet. The viscosity of Loctite 3105 was 300 cP and was printed using pneumatic atomizer of the AJ system. Before printing the structures, ink material was placed in a tube which was rotated continuously around its axis for 12 h using a tube roller (Scilogex MX-T6-S, Rocky Hill, CT, USA) to prevent nanoparticle agglomeration within the ink. UV curable Loctite 3105 was stored without exposure to ambient light prior to printing. A transparent glass slide (Thermo Fisher Scientific, Waltham, MA, USA) was used as the substrate. Prior to printing, the substrates were cleaned in DI water followed by isopropyl alcohol. In order to make the substrate surface hydrophilic and to promote better adhesion of the printed material, the substrate was treated with an atmospheric plasma (Atomflo™ 400, Surfx® Technologies LLC, Redondo Beach, CA, USA) at 100 W for 5 min.

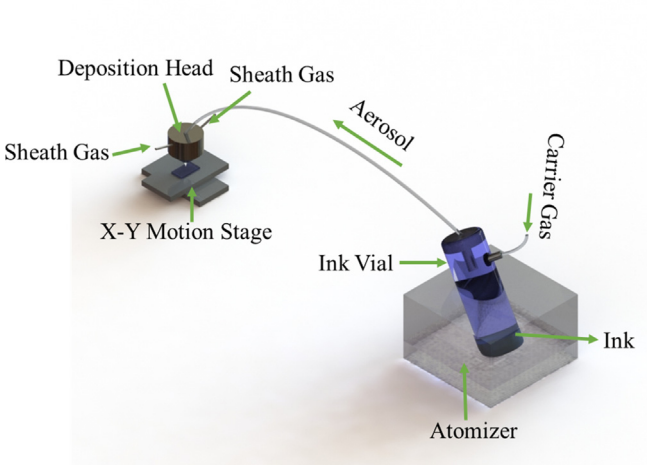

Fig. 1. Schematic of an aerosol jet micro-additive printer.

In the current study, we used both, the ultrasonic and the pneumatic atomizer. The nozzle exit diameter to print the Ag electrode lines was 150 μm (the minimum line width is about 10 times smaller than the nozzle diameter based upon the sheath gas pressure). Three types of nozzle exit diameters, 150 μm, 250 μm, and 300 μm was used to print Loctite 3105 in order to achieve different trace width 30 μm, 100 μm, and 180 μm. While printing, the tip-to-substrate distance was always kept at 3 mm. All other parameters mentioned in Table 1 were optimized for the current work. The details for Ag and polymer printing is presented in following subsections.

a) Additive fabrication of micro electrode: a nanoparticle Ag ink is dispensed on the glass substrate using ultrasonic atomizer in order to fabricate conductive Ag traces at a length scale down to tens of micrometre. Before printing geometry of the conductive part was drawn in AutoCad (Autodesk, 2015) and converted to prg file compatible to the AJ software. The nozzle exit diameter used to print Ag traces was 150 μm. An atomizing flow rate of 25 sccm and a sheath gas flow rate of 50 sccm was used for printing. Width of the printed traces measured by a compound microscope was 15 ± 1.04 μm. The fingers of the sensors including interconnect and probing pad was printed using a single layer of printed material. During printing platen temperature was set to 80 °C.
b) Additive fabrication of micro-scale polymer trace: after printing the conductive silver traces, polymer traces were printed perpendicular to the silver traces in order to create micro electrodes.

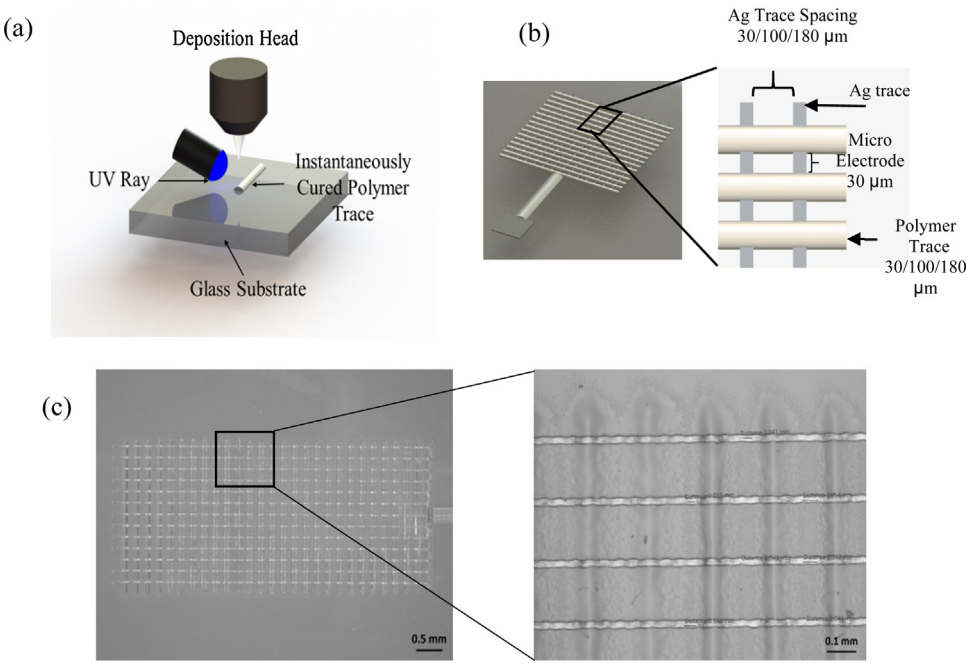

Fig. 2. (a) Schematic showing the fabrication process for microelectrode arrays using an aerosol jet printer. (b) Schematic of microelectrode array. (c) Actual images of AJ printed microelectrode array at different magnifications.

The polymer traces were also created using AutoCAD. Polymer traces were printed with certain distance apart from each other in order to create sensing regions at alternate segments as shown in Fig. 2a–c. Other alternate layers were insulated by polymer layer in order to form the micro electrodes. A UV curable polymer ink was dispensed at an accuracy of tens of micro-meter by a jetting action on top of Ag layers. The polymer ink was instantaneously cured during the dispense using a UV light source as shown in Fig. 2a. With instantaneous curing, it was possible to create solidified polymer layer maintaining the required width. Three different polymer trace widths were used for the three MEAs (see Table 1). By varying different printing parameters, efforts were made to keep micro electrode array width close to 30 μm. During printing, the UV power was set to 30% of the maximum capability (940 mW). Platen temperature for polymer trace printing was 80 °C as well. All completed sensors were thermally sintered in Vulcan 3–550 programmable furnace (Degussa-Ney Dental Inc., Bloomfield, CT, USA) at 100 °C for 15 min followed by air cooling according to manufacturer guideline. Sintering is necessary in order to have conductive electrode lines. The resistivity of the Ag sintered by this method is about 2×10^{-7} Ω-m (manufacturer data sheet), or about an order of magnitude higher than the bulk resistivity.

The exposed silver traces are expected to act as microelectrode arrays. The space between silver trace and the width of the polymer trace define the electrode dimension of the microelectrode arrays. To adjust the space between electrodes, we just print silver traces with different spacing and polymer traces with a different width.

2.2. Chemicals and reagents

Glucose oxidase (GO_x) was used for glucose sensor (Sigma–Aldrich, St. Louis, MO, USA) with an activity of about 185 units mg^{-1}. Hydrogen peroxide (H_2O_2) solution (Sigma Aldrich, St. Louis MO) was stored in refrigerator before use. Nafion solution (5%), hydrogen peroxide (H_2O_2), glutaraldehyde, and β-D-glucose (Sigma–Aldrich, St. Louis MO) used in this work were available with analytical grade purity. The stock solution of Nafion, H_2O_2 and glutaraldehyde were stored in refrigerator before use. Electrochemical measurements were carried out in a 0.1 M phosphate buffer solution (PBS) (pH = 7.4). All aqueous solutions were prepared using deionized water (18 MΩ cm). Certain stock concentrations of glucose (mutarotation was allowed for at least 12 h) were prepared in the buffer solution and stored at 4 °C.

2.3. Electrochemical analysis instrumentation

Cyclic voltammetry (CV) and Chronoamperometric (CA) measurements were performed by using CHI 660E electrochemical workstation (CH Instruments Inc., Austin, TX, USA). A three electrode cell had platinum wire (ø 0.5 mm, CHI115, from CH Instruments Inc.) as a counter electrode and a saturated calomel reference electrode (SCE, CHI150, from CH Instruments Inc.) was used for electrochemical measurements. During the CV measurement,

Table 1
Variables to create different types of sensor.

Sensor types	Ag trace width (μm)	Dist. between Ag trace (μm)	Nozzle used for Ag trace (μm)	Sheath gas/UA atm. flow rate (sccm)	Polymer trace width (μm)	Nozzle tip diameter used for polymer trace (μm)	Micro electrode width (μm)	Sheath gas/PA Atm/exhaust flow rate (sccm)
1	15 ± 1.04	30	150	50/25	30.36 ± 1.55	150	31.06 ± 2.40	60/630/625
2	15 ± 1.04	100	150	50/25	99.75 ± 1.35	250	31.74 ± 3.60	85/725/735
3	15 ± 1.04	180	150	50/25	178.95 ± 4.36	300	30.25 ± 2.72	80/710/740

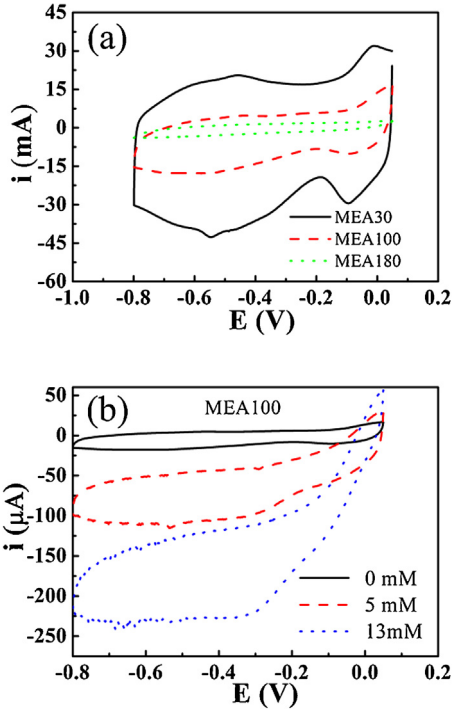

Fig. 3. (a) Cyclic voltammetry of three electrodes (MEA30, MEA100, MEA180) in PBS solution; (b) MEA100 in different concentrate ion of H_2O_2 solution (0, 5, 13 mM). The scan rate is 100 mV s^{-1} and the reference electrode is SCE.

initial potential was 0.0 V, and the initial scan direction was negative. All experiments were conducted at room temperature (about 26 °C).

2.4. Formulation of microelectrode array biosensor (MEAB)

Silver MEA was chosen as the base electrode. A 5 μL drop of glucose oxidase solution (5.4 mg mL^{-1}) was dried on the MEA electrode at room temperature. The enzyme-modified electrode was coated with 5.0 μL of 0.5% Nafion solution. A 3.0 μL of glutaraldehyde (1%) was dropped on the resulting electrode and dried for 1–2 h. The resulting microelectrode array biosensor (MEAB) was washed with phosphate buffer (0.1 M, pH 7.4) and stored at 4 °C.

3. Results and discussion

3.1. Electrochemical behavior of the as-prepared MEA

Hydrogen peroxide (H_2O_2) and glucose are two important analytes/biomarkers [25,26]. H_2O_2 is the simplest peroxide, an oxidizer commonly used as bleach, and also a by-product of many oxidase (such as glucose oxidase, lactate oxidase) catalytic reactions. Further, the H_2O_2 concentration is proportional to the concentration of the enzymatic analytes. Thus concentration of these analytes/biomarkers can be measured by assessing the concentration of H_2O_2.

Cyclic voltammetry (CV) was conducted in PBS and hydrogen peroxide solution at 100 mV s^{-1}. During the measuring process, the MEA were dipped into the solution. Since the connection part of the electrode is covered by printed polymer, it will not be exposed to the solution and does not influence the area of the electrode. Fig. 3a shows the CV curves of three electrodes with different electrode spacing: 30 μm (MEA30); 100 μm (MEA100); and 180 μm (MEA180). It was observed that, with the increase of Ag trace spacing, double layer charging current (IC) of the electrodes decreased dramatically. The double layer charging current (IC) is proportional

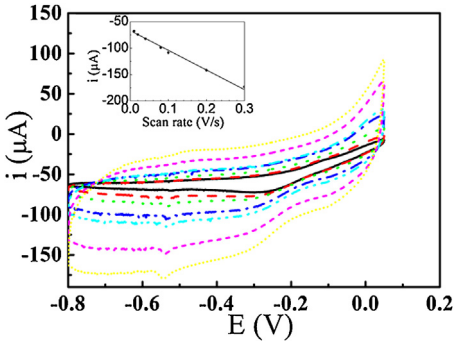

Fig. 4. Cyclic voltammograms of MEA100 in 5 mM H_2O_2 solution with scan rates of: 10, 20, 40, 80, 100, 200 and 300 mV s^{-1}. The inset shows the fitting curves of peak current vs. sweep rate (ν).

to active area of the electrode. MEA30 has the largest charging current and MEA180 has the lowest charging current corresponding to the reduction of electrode areas with increasing trace spacing. These results prove the efficacy of the microelectrode arrays.

Fig. 3b shows the CV curves of MEA100 for different concentrations of hydrogen peroxide solution. The resulting electrodes exhibit good electrocatalysis towards the reduction of H_2O_2. The onset reduction potential is about 0 V, which is more positive and echoes the good electroreduction ability of the MEA100 electrode. The reduction current reaches maximum at about −0.3 V and maintains an almost constant value till −0.8 V. We choose −0.6 V as an applied potential in most cases. In absence of H_2O_2, the reducing current is low, only about 17 μA at −0.6 V vs. SCE (the lower lines of the CV cycle). With the increasing amount of H_2O_2 to 5 mM and 13 mM, the reduction current also increased to about 110 μA and 230 μA, respectively, which clearly shows the reduction ability of the silver electrode towards hydrogen peroxide. The dramatic increase of reduction currents is caused by the electroreduction effect of the silver electrode towards hydrogen peroxide. Such a signal justifies the choice of silver nanoparticles to fabricate MEAs to detect H_2O_2. We will show the detailed detection process in chronoamperometric measurement part.

Fig. 4 shows cyclic voltammogram curves of MEA100 as representative of MEAs in 5 mM H_2O_2 solution with sweep rate 10, 20, 40, 80, 100, 200 and 300 mV s^{-1} (from inner ring to outer ring). The reducing current at −0.6 V is chosen as cathode peak current since the cathode reducing current is almost at the maximum value at this potential. The inset shows the corresponding fitting curves of peak current versus sweep rate (ν). As the theory predicted, the linear relation between peak current and sweep rate indicates that the kinetic behavior of the electrode reaction is dominated by surface electrochemistry reaction, while the linear relation between peak current and the square root of sweep rate indicates a surface diffusion controlled electrode reaction. In this case, the peak current versus the sweep rate plot was linear ($R = 0.99$), implying that the kinetic behavior of the electrode is not surface diffusion controlled process rather a surface-confined electrode reaction [25,27].

The chronoamperometric (CA) curves of MEA100 for different concentration of H_2O_2 solutions (from top to bottom, the curves correspond to 0, 0.2, 0.5, 1.0, 3.0, 5.0, 7.0, 9.0, 11.0, 13.0, 15.0, 17.0, 19.0, 21.0, 25.0,29.0 and 37.0 mM, respectively) are shown in Fig. 5. During CA measurement, the initial potential is set as −0.1 V, the high potential is set as 0.05 V, and the low potential is set to be −0.6 V. The pulse width was set to 120 s. With the increasing concentration of H_2O_2, the reduction current increases linearly. The CA analysis of MEA30 and MEA180 were also performed for different concentration of H_2O_2. Plot for MEA100 is shown as a representative plot. The i–c curves were plotted with the concentration of H_2O_2 and the corresponding current value at 240 s of the CA curves.

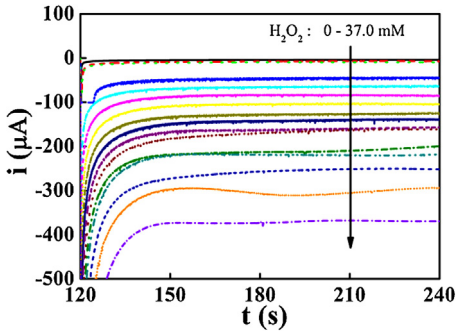

Fig. 5. The chronoamperometric (CA) curves (measured with high potential 0.05 V and low potential −0.6 V vs. SCE) of MEA100 with different concentration of H_2O_2 (from top to bottom, the curves correspond to 0, 0.2, 0.5, 1.0, 3.0, 5.0, 7.0, 9.0, 11.0, 13.0, 15.0, 17.0, 19.0, 21.0, 25.0,29.0 and 37.0 mM of H_2O_2, respectively).

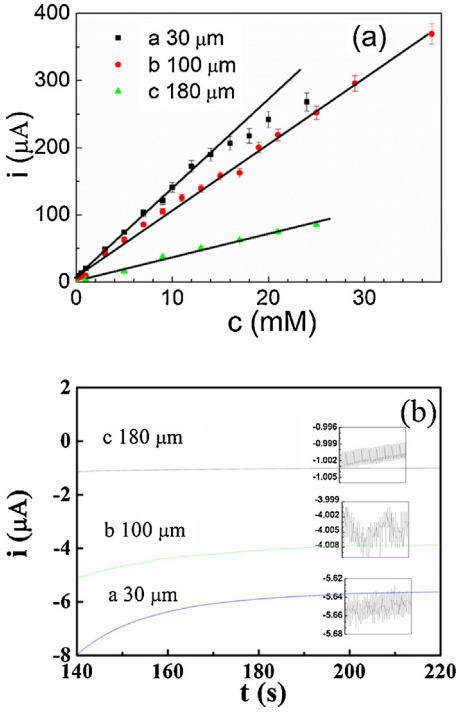

Fig. 6. (a) i–c curves of the three electrodes (MEA30, 100 and 180) derived from CA measurements of H_2O_2, and (b) noise of three microelectrodes with different Ag trace spacing.

The i–c curves of MEA30, MEA100 and MEA180 are shown in Fig. 6a. All printed electrodes showed linear behavior for certain H_2O_2 concentration range. With increasing Ag trace spacing, the sensitivity (slope of the linear part) decreased. MEA 30 worked linearly in H_2O_2 solution with a concentration range between 0.2 mM and 14.0 mM. The corresponding regression equation of the linear plot was: $I/\mu A = 7.5 + 13.3\,c$, $N = 9$, $R = 0.998$, where c is the concentration of H_2O_2 in mM. The sensitivity was estimated to be 13.3 μA mM^{-1}. While for MEA100 and MEA180, the linear range was larger. The MEA100 has a linear range over 37 mM and MEA 180 over 25 mM. Higher concentrations could not be measured due to delamination of electrode with very high H_2O_2 concentration. The corresponding regression equations for MEA100 and MEA180 are $I/\mu A = 5.1 + 9.9\,c$, $N = 17$, $R = 0.996$ and $I/\mu A = 1.1 + 3.6\,c$, $N = 9$, $R = 0.991$, respectively (c is the concentration of H_2O_2 in mM). The sensitivities are 9.9 μA mM^{-1} and 3.6 μA mM^{-1} for MEA100 and MEA180, respectively. With the increase of Ag trace spacing, the response current towards the same H_2O_2 concentration was decreased due to the decrease of number of the microelectrodes and thus decrease in active areas. However, with the increase of Ag trace spacing, the noise level of the electrodes decreased drastically as shown in Fig. 6b. The noise of MEA30 is 12 nA, while for MEA100 and MEA180 noise were 1.5 and 1.2 nA for the same measurement condition. The detection limit was then calculated ($S/N = 3$) to be 2.7 μM, 0.45 μM and 1.0 μM, respectively. The MEA100 electrode has the lowest detection limit.

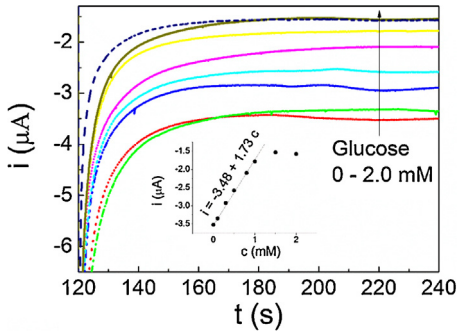

Fig. 7. The chronoamperometric (CA) curves of MEA100 glucose sensor with different concentration of glucose (from bottom to up, 0 to 2 mM). The inset shows the i–c curve of glucose derived from CA measurements.

Note that the MEAs were 2.0 mm in width and 6.0 mm in length, and each microelectrode has almost the same dimension, having 15 μm width and 30 μm length. As a result, the total number of microelectodes of MEA30, MEA100 and MEA180 is about 4400, 803 and 297, respectively. The total electrodes area of a MEA is proportional to its total number of microelectrodes. The electrodes area of MEA30:MEA100:MEA180 is calculated to be 14.8:2.7:1. The sensitivity of the three MEAs is 13.3, 9.9 and 3.6 μA mM^{-1}, which is almost 3.7:2.8:1. As to MEA100 and MEA180, the response current is proportional to the total electrodes area. However, as to the MEA30, compared with its total electrodes area, the response current is much lower than it should be. The current density of MEA30, MEA100 and MEA180 is 0.67, 2.74 and 2.60 mA cm^{-2} mM^{-1}, respectively, which is almost 0.25:1:1. This clearly shows that MEA30 suffers from diffusion layer overlap with its neighboring electrodes, while MEA100 and MEA180 have sufficiently separated microelectrodes to avoid any issues. The results directly prove that the electrode density (which is inversely proportion to Ag trace spacing) plays an important role in microelectrode arrays [1]. Compared with other fabrication methods, micro additive manufacturing has great advantage to fabricate adjustable microelectrode arrays with controlled electrode density, especially for rapid prototyping.

3.2. *The performance of the electrode as a glucose biosensor*

Glucose oxidase (GO_x) was chosen as a model enzyme immobilized on the MEA100 electrode with glutaraldehyde and Nafion to make a micro-electrode array biosensor (MEAB). The chronoamperometric (CA) measurement were carried out to detect glucose. During the CA measurement, the high potential was set at 0.05 V and the low potential was set at −0.6 V vs. SCE, the pulse width was setting to be 120 s. As shown in Fig. 7, with the increase of glucose concentration, the absolute value of response current decreased because of exhaustion of oxygen [25].

The i–c curves of glucose derived from CA measurements is shown in the inset of Fig. 7. The MBA sensor worked linearly in glucose solution in the concentration range from 0.1 mM to 1.0 mM. The corresponding regression equation of the linear plot was: $I/\mu A = -3.48 + 1.73\,c$, $N = 6$, $R = 0.99$, where c is the concentration of glucose in mM. The sensitivity is 1.73 μA mM^{-1} while the calculated value of detection limit ($S/N = 3$) is 1.7 μM. The above results

clearly demonstrate the feasibility of using additively fabricated MEAs for biosensing application.

4. Conclusion

In this work, microelectrode arrays with adjustable electrode spacing are fabricated using aerosol jet micro additive manufacturing method. The dimension of each individual electrode is about $15 \times 30\ \mu m^2$. The space between Ag traces is controlled to be about 30 μm (MEA30), 100 μm (MEA100) and 180 μm (MEA180), respectively. Hydrogen peroxide and glucose were chosen as analytes to justify the performance of the MEAs. The electrodes can reduce hydrogen peroxide and the reduction current is proportional to the concentration of hydrogen peroxide in wide concentration ranges. Though MEA30 has the highest sensitivity ($13.3\ \mu A\ mM^{-1}$), its detection limit is also high (2.7 μM) due to the highest noise level (12 nA). The MEA180 has the lowest noise level (1.2 nA) but its detection limit (1.0 μM) is not the lowest due to its lower sensitivity ($3.6\ \mu A\ mM^{-1}$). The MEA100 has a relatively high sensitivity ($9.9\ \mu A\ mM^{-1}$) and low noise level (1.5 nA), therefore its detection limit is the lowest (0.45 μM). The current density of MEA30, MEA100 and MEA180 is 0.67, 2.74 and 2.60 $mA\ cm^{-2}\ mM^{-1}$, respectively. The results clearly show that MEA30 suffers from diffusion layer overlap with its neighboring electrodes, while MEA100 and MEA180 have sufficiently separated microelectrodes to avoid any overlap of diffusion layers. GO_x was chosen as a model enzyme immobilized on the MEA100 to show its biosensing ability. This work opens up an easy, quick, low-cost and environmentally friendly micro additive manufacturing method to fabricate high performance microelectrode arrays. It can be used as an electrochemical platform for a wide range of applications such as biosensors, biofuel cells and other electrochemical devices.

Acknowledgments

This work was supported by RP's startup fund. HY gratefully acknowledge the financial support from Shenzhen Science and Technology Research Grant (JCYJ20150324140036855) and Guangdong Natural Science Foundation (2015A030313545). DD and YL would like to acknowledge the financial support from the Centers for Disease Control and Prevention/National Institute for Occupational Safety and Health (CDC/NIOSH) Grant No. R21OH010768. Its contents are solely the responsibility of the authors and do not necessary represent the official views of CDC. Author would like to thank Yang Song for his helpful discussion in sensor design.

References

[1] B.R. Scharifker, Diffusion to ensembles of microelectrodes, J. Electroanal. Chem. 240 (1988) 61–76.
[2] Y.H. Lin, F. Lu, Y. Tu, Z.F. Ren, Glucose biosensors based on carbon nanotube nanoelectrode ensembles, Nano Lett. 4 (2004) 191–195.
[3] S.K.J. Ludwig, C. Tokarski, S.N. Lang, L.A. van Ginkel, H.Y. Zhu, A. Ozcan, et al., Calling biomarkers in milk using a protein microarray on your smartphone, PLoS One 10 (2015) e0134360.
[4] D.A. Armbruster, M.D. Tillman, L.M. Hubbs, Limit of detection (Lod) limit of quantitation (Loq)—comparison of the empirical and the statistical, methods exemplified with Gc–Ms assays of abused drugs, Clin. Chem. 40 (1994) 1233–1238.
[5] W.E. Morf, N.F. de Rooij, Performance of amperometric sensors based on multiple microelectrode arrays, Sens. Actuators B: Chem. 44 (1997) 538–541.
[6] I.F. Cheng, L.D. Whiteley, C.R. Martin, Ultramicroelectrode ensembles—comparison of experimental and theoretical responses and evaluation of electroanalytical detection limits, Anal. Chem. 61 (1989) 762–766.
[7] Y. Tu, Y.H. Lin, Z.F. Ren, Nanoelectrode arrays based on low site density aligned carbon nanotubes, Nano Lett. 3 (2003) 107–109.
[8] J.M. Hinzman, J.L. Gibson, R.D. Tackla, M.S. Costello, J.J. Burmeister, J.E. Quintero, et al., Real-time monitoring of extracellular adenosine using enzyme-linked microelectrode arrays, Biosens. Bioelectron. 74 (2015) 512–517.
[9] M.D. Graaf, K.D. Moeller, Introduction to microelectrode arrays, the site-selective functionalization of electrode surfaces, and the real-time detection of binding events, Langmuir 31 (2015) 7697–7706.
[10] X.W. Du, L. Wu, J. Cheng, S.L. Huang, Q. Cai, Q.H. Jin, et al., Graphene microelectrode arrays for neural activity detection, J. Biol. Phys. 41 (2015) 339–347.
[11] M. De Leo, F.C. Pereira, L.M. Moretto, P. Scopece, S. Polizzi, P. Ugo, Towards a better understanding of gold electroless deposition in track-etched templates, Chem. Mater. 19 (2007) 5955–5964.
[12] M.A. Guillorn, T.E. McKnight, A. Melechko, V.I. Merkulov, P.F. Britt, D.W. Austin, et al., Individually addressable vertically aligned carbon nanofiber-based electrochemical probes, J. Appl. Phys. 91 (2002) 3824–3828.
[13] R. Intartaglia, S. Beke, M. Moretti, F. De Angelis, A. Diaspro, Fast and cost-effective fabrication of large-area plasmonic transparent biosensor array, Lab Chip 15 (2015) 1343–1349.
[14] J.C. Claussen, A.D. Franklin, A. ul Haque, D.M. Porterfield, T.S. Fisher, Electrochemical biosensor of nanocube-augmented carbon nanotube networks, Acs Nano 3 (1) (2009) 37–44.
[15] M. Zangheri, L. Cevenini, L. Anfossi, C. Baggiani, P. Simoni, F. Di Nardo, et al., A simple and compact smartphone accessory for quantitative chemiluminescence-based lateral flow immunoassay for salivary cortisol detection, Biosens. Bioelectron. 64 (2015) 63–68.
[16] A. Roda, E. Michelini, L. Cevenini, D. Calabria, M.M. Calabretta, P. Simoni, Integrating biochemiluminescence detection on smartphones: mobile chemistry platform for point-of-need analysis, Anal. Chem. 86 (2014) 7299–7304.
[17] C.M.B. Ho, S.H. Ng, K.H.H. Li, Y.J. Yoon, 3D printed microfluidics for biological applications, Lab Chip 15 (2015) 3627–3637.
[18] R. Liu, H.Y. Ding, J. Lin, F.P. Shen, Z. Cui, T. Zhang, Fabrication of platinum-decorated single-walled carbon nanotube based hydrogen sensors by aerosol jet printing, Nanotechnology 23 (2012) 505301.
[19] F.X. Wang, J. Lin, W.B. Gu, Y.Q. Liu, H.D. Wu, G.B. Pan, Aerosol-jet printing of nanowire networks of zinc octaethylporphyrin and its application in flexible photodetectors, Chem. Commun. 49 (2013) 2433–2435.
[20] E. Jabari, E. Toyserkani, Micro-scale aerosol-jet printing of graphene interconnects, Carbon 91 (2015) 321–329.
[21] W. Zhu, J.X. Li, Y.J. Leong, I. Rozen, X. Qu, R.F. Dong, et al., 3D-printed artificial microfish, Adv. Mater. 27 (2015) 4411–4417.
[22] J.R. Tumbleston, D. Shirvanyants, N. Ermoshkin, R. Janusziewicz, A.R. Johnson, D. Kelly, et al., Continuous liquid interface production of 3D objects, Science 347 (2015) 1349–1352.
[23] M.T. Rahman, L. Renaud, D. Heo, M.J. Renn, R. Panat, Aerosol based direct-write micro-additive fabrication method for sub-mm 3D metal-dielectric structures, J. Micromech. Microeng. 25 (2015) 107002.
[24] M.T. Rahman, A. Rahimi, S. Gupta, R. Panat, (2016) Submitted for publication.
[25] C.S. Shan, H.F. Yang, J.F. Song, D.X. Han, A. Ivaska, L. Niu, Direct electrochemistry of glucose oxidase and biosensing for glucose based on graphene, Anal. Chem. 81 (2009) 2378–2382.
[26] H.P. Yang, Y.F. Zhu, D.C. Chen, C.H. Li, S.G. Chen, Z.C. Ge, Electrochemical biosensing platforms using poly-cyclodextrin and carbon nanotube composite, Biosens. Bioelectron. 26 (2010) 295–298.
[27] H.P. Yang, Y.F. Zhu, Glucose biosensor based on nano-SiO2 and unprotected Pt nanoclusters, Biosens. Bioelectron. 22 (2007) 2989–2993.

Biographies

Haipeng Yang is an associate professor at the College of Materials Science and Engineering at SZU. He received his BS and MS in chemistry from Lanzhou University, and PhD from Institute of Physics, Chinese Academy of Sciences. He joined Shenzhen University in 2006. Currently he is a visiting scholar at Washington State University. His research interests include functional nanomaterials for electrochemical biosensing and fuel cells.

Md Taibur Rahman is a PhD student in the School of Mechanical and Materials Engineering at the Washington State Univerty. He received his MS degree from the University of Texas at El Paso and BS degree from the Chittagong University of Engineering and Technology. He has several papers to his credit in the areas of ceramics and additive manufacturing.

Dan Du received her Ph.D. in Analytical Chemistry from Nanjing University in 2005. She joined Central China Normal University in 2005 and was promoted to Full Professor in 2011. Currently she is a Research Professor at Washington State University. Her research interests include functional nanomaterials for fuel cells and electrochemical biosensing.

Rahul Panat is an associate professor at the School of Mechanical and Materials Engineering at WSU. He received his MS in Mechanical Engineering from the University of Massachusetts, Amherst, and his PhD from the University of Illinois at Urbana-Champaign in Theoretical and Applied Mechanics. He worked at Intel's manufacturing R&D from 2004–2014 before joining WSU in Fall 2014. At Intel, Dr. Panat worked on lead-free conversion of flash memory processors, fine line-space PCB development, and ceramic capacitors and their integration in IC chips. Dr. Panat also worked as an adjunct faculty at the Arizona State University from 2012–2014 in the area of flexible Li-ion batteries. Dr. Panat leads the Advanced Manufacturing Laboratory at WSU with concentration in the areas of printed and flexible electronics,

packaging, 3-D mm wave antennas, and Li-ion batteries. Dr. Panat is the recipient of several awards including a Gold Medal from MRS, and several Divisional Recognition Awards at Intel, including one for his work on the first halogen-free chip.

Yuehe Lin is a professor at Washington State University and a Laboratory Fellow at Pacific Northwest National Laboratory. His research interests include electrochemistry, bioanalytical chemistry, chemical sensors and biosensors, fuel cells and batteries, material synthesis and applications. He has over 10 patents and has published about 350 papers, with total citation ~25,000, H-index 84. He is a fellow of the American Association of the Advancement of Science (AAAS), the Royal Society of Chemistry of the UK, and the American Institute for Medical and Biological Engineering (AIMBE).